Manuscript ID 2024-CDPA-0542

Estimation of Participation Factors for Power System Oscillation from Measurements

Tianwei Xia, *Member, IEEE*, Zhe Yu, *Senior Member, IEEE*, Kai Sun, *Fellow, IEEE*, Di Shi, *Senior Member, IEEE,* Kaiyang Huang, *Student Member, IEEE*

***Abstract*—In a power system, when the participation factors of generators are computed to rank their participations into an oscillatory mode, a model-based approach is conventionally used on the linearized system model by means of the corresponding right and left eigenvectors. This paper proposes a new approach for estimating participation factors directly from measurement data on generator responses under selected disturbances. The approach computes extended participation factors that coincide with accurate model-based participation factors when the measured responses satisfy an ideally symmetric condition. This paper relaxes this symmetric condition with the original measurement space by identifying and utilizing a coordinate transformation to a new space optimally recovering the symmetry. Thus, the optimal estimates of participation factors solely from measurements are achieved, and the accuracy and influencing factors are discussed. The proposed approach is first demonstrated in detail on a two-area system and then tested on an NPCC 48-machine power system. The penetration of inverter-based resources is also considered.**

***Index Terms*—Dynamic response, Measurement-based approach, Participation factors, Power system oscillations.**

I. Background

In an interconnected power system, rotor angle oscillations among generators are prevalent, as evidenced by real-time wide-area measurements under both ambient and contingency conditions. Such oscillations, especially low-frequency inter-area oscillations, can affect the safety margins for grid operations [1] and cause stability issues of generators [2]. The Participation Factor (PF), as a useful small-signal analysis tool, can evaluate how each state variable of a generator or dynamic device participates in an oscillatory mode [3]. PFs of state variables regarding a specific oscillatory mode, i.e., a pair of complex eigenvalues, are conventionally calculated as the products of corresponding elements from both the right and left eigenvectors of the system's linearized model. Comparatively, the mode shape and mode composition as another two modal properties focus only on one-way linkages between state variables and the mode by utilizing either the right or left eigenvector. Thus, a PF captures both the response of a state variable with the mode, i.e., the mode shape, and its contribution to the mode, i.e., the mode composition, evaluating a bidirectional connection between the state variable and mode.

Accurate estimation of PFs can largely benefit grid operations in the real-time environment. For instance, when an oscillation occurs, knowing how generators participate in the oscillation mode can pinpoint the most involved or susceptible generators for early mitigation before instability is caused. The generators with high PFs can be the candidate locations to perform damping control using Power System Stabilizers (PSS) [3]. Recently, PFs have also been applied to renewable energy systems for the identification of crucial state variables in phase-locked loops [4-6] and DC links [7] associated with sub-synchronous oscillations. Furthermore, PFs are used to associate oscillation damping with generator outputs for strategic generation re-dispatches [8][9].

For practical applications, variant linear PFs have been proposed to satisfy different application demands. For instance, reference [10] introduces loop participation factors that evaluate the influences of individual components on system modes by leveraging the loop and nodal observability and controllability. Reference [11] proposes impedance participation factors to analyze the sensitivity of black box models, defined in terms of the residue of the whole-system admittance matrix with the chain rule. A similar impedance participation factor is discussed in [12], focusing on frequency domain performance. In addition, a recent study in [13] advances modal PFs for exploring the role of algebraic variables in modes more comprehensively.

Alternative methodologies and definitions for PFs have been explored extensively in literature [14]-[22], where the classic PF concept based on the state matrix has been expanded through perspectives of probability and nonlinearity. Reference [17] broadens the PF definition to correlate with the initial system state, enabling PFs to represent an average connection between a state variable and a mode across responses from various initial states. This "extended PF" has been validated against traditional model-based PFs, contingent on the distribution of initial states fulfilling an ideally symmetric condition. The advantages of these extended PFs in power systems are illustrated in [18] and [19]. References [20] and [21] distinguish between mode-in-state PFs and state-in-mode PFs, using a model-based calculation approach that

This work was supported by the NSF grant ECCS-2329924.

T. Xia, K. Sun, and K. Huang are with the Department of EECS, University of Tennessee, Knoxville, TN 37996 USA (e-mail: tianweixia@gmail.com, kaisun@utk.edu, khuang12@vols.utk.edu).

Z. Yu is with Ant Group, Hangzhou, China (e-mail: yzae2623@gmail.com).

D. Shi is with the ECE Department, New Mexico State University, Las Cruces, NM 88003 USA (e-mail: dshi@nmsu.edu).

relies on eigenanalysis on the system's linearized model. Another study [22] examines the uniqueness of the extended PF and introduces the energy-based PF as an alternative.

Conventionally, PFs are calculated from a system's linearized model. Most existing methods presume access to all right (or left) eigenvectors of the linearized model. However, a linearized model for the whole power grid is not always available in practice, especially with high inverter-based resource penetration [23]. An alternative method involves using wide-area measurements to monitor the responses of generators and other dynamic devices to small disturbances, thus enabling the estimation of their PFs directly from measurement data. However, there is limited research on measurement-based PF estimation for power systems. Reference [24] employs a Koopman operator-based approach for measurement-based PFs and allows for estimating both linear and nonlinear PFs within the Koopman mode. This approach relies on the choice of the observable function, which is a question still unresolved in the field [25]. Reference [26] also determines PFs from measurement data, where the PFs are estimated by certain perturbation on the desired variables; however, the response-based PF method in [26] requires carefully designing the perturbation on the black-box model. Specifically speaking, it involves perturbing a specific state variable, such as the rotor angle of a particular generator, while keeping other state variables unchanged, which means that this approach assumes full controllability of the system and significantly limits its practical use.

Although there are limited papers specifically addressing participation factor estimation from measurements, oscillation mode identification has been a popular topic in recent decades. Various methods have been proposed and developed, including Prony analysis [27-29], Kalman filtering [30, 31], discrete Fourier transform (DFT) [32], wavelet transform [33], and others. Prony analysis is widely used in power systems to obtain mode shapes and frequencies [27]. It has been generalized or modified for specific applications such as harmonic analysis [28] or nonlinear analysis [29]. The DFT method converts a finite signal sequence into a same-length sequence in the frequency domain [30], commonly used for frequency identification. Kalman filtering is an algorithm that estimates unknown variables and is particularly effective in dealing with statistical noise [32]. Wavelet transform, on the other hand, decomposes signals into oscillations over time and frequency, making it suitable for analyzing mode properties in the time domain [33].

This paper is dedicated to estimating the linear PFs of generators within oscillatory modes directly from measurement data and proposes a practical methodology. The key contributions of the paper include: 1) a systematic approach to computing PFs from measurement data, which uses extended PFs as a bridge but relaxes the symmetric condition by finding a coordinate transformation; 2) a PF estimation methodology applicable to black-box models by generalizing response-based PFs in [27]; 3) demonstration and validation of the new approach on a large-scale model considering the penetration of inverter-based resources (IBRs).

The rest of the paper is organized as follows: Section II details the proposed measurement-based approach, including the determination of coordinate transformations for optimal state space symmetry, the computation of extended PFs, and the method of translating these calculated PFs back to the original state space. In Section III, the proposed method is initially applied to a two-area system and later tested on a 48-machine Northeastern Power Coordinating Council (NPCC) model. Conclusions are drawn in Section IV.

II. Proposed Measurement-based PF Estimation Method

A. Preliminary

Consider an N-dimensional linear system in (1) describing a power system model linearized at its stable equilibrium:

$$\dot{\mathbf{x}} = \mathbf{A}\mathbf{x}\,. \tag{1}$$

Let λ_i denote the i-th eigenvalue of matrix $\mathbf{A}$. Its left eigenvector $\boldsymbol{\psi}_i=[\psi_{i1}, \ldots \psi_{iN}]$ and right eigenvector $\boldsymbol{\phi}_i=[\phi_{1i}, \ldots \phi_{Ni}]^{\mathrm{T}}$ respectively define the composition and shape of the mode. Note that if λ_i is complex, it and its conjugate together define one oscillatory mode of matrix $\mathbf{A}$, referred to as mode i. Since the eigenvectors are also conjugates and convey identical information, modal properties can be investigated based on either λ_i or its conjugate. Then, the PF of the k-th state in mode i is defined by

$$\mathrm{PF}_{ki} \overset{\text{def}}{=} p_{ki} = \psi_{ik}\phi_{ki}\ , \tag{2}$$

as a dimensionless value. Notice that (2) provides a general model-based approach to calculate PF from the shape ϕ_{ki} and composition ψ_{ik} of the mode.

When an accurate matrix $\mathbf{A}$ is unavailable, PFs can still be estimated as follows. The response of the k-th state variable subject to a small disturbance can be written as a combination of N modes

$$x_k(t) = \sum_{i=1}^{N} B_{ki} e^{\lambda_i t} = \sum_{i=1}^{N} (\boldsymbol{\psi}_i \mathbf{x}_0)\phi_{ki} e^{\lambda_i t} \quad (k=1, \ldots, N), \tag{3}$$

where $\mathbf{x}_0 = [x_{01},\ldots, x_{0N}]^{\mathrm{T}}$ is the initial state vector, and modal amplitude $B_{ki}= \boldsymbol{\psi}_i\mathbf{x}_0\phi_{ki}$ is proportional to the mode shape ϕ_{ki}, which evaluates how much mode i is excited in the k-th state variable. From state responses, ϕ_{ki} can be estimated by normalizing amplitude B_{ki} with respect to the initial condition $\mathbf{x}_0$ [34]. Accordingly, paper [17] proposes Extended Participation Factors (EPFs) defined by (4), utilizing all state responses starting from a set of initial states:

$$\mathrm{EPF}_{ki} \overset{\text{def}}{=} \underset{\mathbf{x}_{k0}^{(l)} \in S}{avg} \frac{B_{ki}^{(l)}}{x_{k0}^{(l)}}, \tag{4}$$

where S is the compact set of the initial values of the, and "(l)" indicates the element index of the set S. It has been proved that EPFs are equivalent to conventional participation factors when initial states satisfy a symmetric condition (defined below). Since B_{ki} can be derived from measured responses via data-driven modal analysis, this extension facilitates the direct estimation of PFs from measurement data. The information on mode i, including contribution factors and damping ratio, is determined using a measurement-based approach applied to the system's response data. In this paper, the Prony method is adopted, which fits a time window of the system response.

Regarding the state variable index k, this paper assumes that the state variables are measurable, and their related information can be obtained from measurement devices.

To avoid any confusion, (4) is designated as the EPF for clarity, following the terminology used in references [18] and [19]. Notably, this term is referred to by a different name in reference [17].

A *symmetric condition* in [17] refers to the symmetry of the initial state set S in the view of any dimension. In other words, for any $k \in \{1, 2, \ldots, N\}$, any state $z = (z_1, \ldots, z_k, \ldots, z_N) \in S$ implies $(z_1, \ldots, -z_k, \ldots, z_N) \in S$. Suppose the initial state set S satisfies this symmetric condition in the state space. In that case, the state variables' distribution exhibits independence, and then the EPFs are equal to conventional PFs calculated from eigenvectors. This can be proved as:

$$\mathrm{EPF}_{ki} = \psi_{ik}\phi_{ki} + \frac{1}{L}\sum_{l=1}^{L}\sum_{j=1,j\neq k}^{N}\psi_{jk}\phi_{ki}\frac{x_{j0}^{(l)}}{x_{k0}^{(l)}} = \psi_{ik}\phi_{ki} = \mathrm{PF}_{ki}, \quad (5)$$

where N is the system dimension, and L is the total number of the initial state set. Variable $x^{(l)}_{j0}$ denotes the j-th state for element l. Consider a 2-dimensional system where the four initial states form a rectangle in the state space, representing ideal symmetry (as shown in the bottom right figure of Fig. 1). Under this condition, the EPFs are the same as the PFs.

B. Idea of the new approach

However, when a power system experiences oscillations subjected to a disturbance, the collected field measurements may not necessarily satisfy this symmetric condition. This paper introduces a new measurement-based approach for

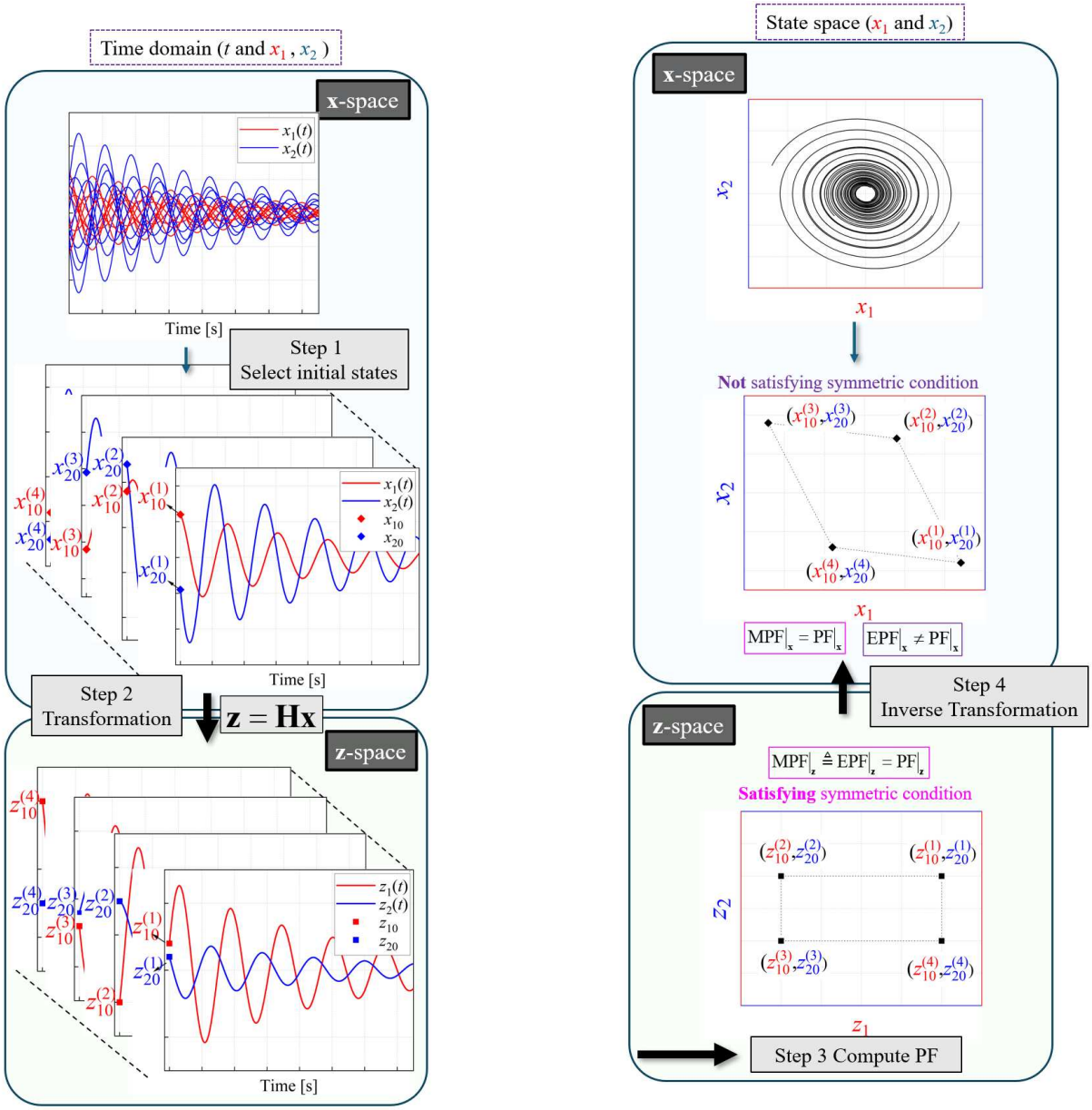

Fig. 1. Structure of new measurement-based approach. (**PF**: Participation factors, **MPF**: Measurement-based PF, **EPF**: Extended PF)

calculating PFs even when the symmetry condition is not satisfied, as illustrated in Fig. 1.

Above all, two assumptions need to be clarified. This paper focuses on studying linear system oscillations, assuming that the system is stable around equilibrium points. In other words, all oscillation modes have a negative damping ratio. The main assumptions are: 1) The system's nonlinearity must be relatively small. 2) The system's perturbations should not be too large.

The idea of the new approach is to introduce a linear transformation **H**, which maps the original state space on **x** into a new state space on **z**. It is expected that in this transformed **z**-space, selected measurement data can exhibit the most symmetric distribution, enabling the EPFs computed using (4) to best approximate the true PFs in **z**-space. Subsequently, the calculated EPFs in **z**-space are transformed back to the original **x**-space, ultimately providing estimates of PFs. In this paper, the PFs estimated from measurements using the proposed method are referred to as Measurement-based Participation Factors or MPFs for brevity.

To avoid ambiguity, TABLE I presents detailed information about the three types of PFs studied in this paper. In the rest of Section II, the four steps of the proposed approach are detailed, followed by a discussion on errors in PF estimation.

TABLE I THE DIFFERENCE BETWEEN DIFFERENT KINDS OF PFS

Name	Formula	Data Source	Description
PF	(2)	Model-based	Based on the PF definition
EPF	(4)	Model or measurement-based	Equal to PF under the symmetric condition
MPF	(3)	Measurement -based	Applying EPF as the bridge for the optimal estimate of PF from measurements

The steps are as follows:

Step 1: Select the optimal set of initial states from measurements.

Step 2: Find the transformation **H** toward a **z**-space to best meet the symmetric condition.

Step 3: Compute the MPFs in **z**-space.

Step 4: Translate the MPFs back to **x**-space.

1) Step 1 Selecting the optimal set of initial states

In *D*-dimensional state space, a set of initial states satisfying the symmetric condition has a symmetric distribution and appears as symmetrical pairs around the equilibrium, i.e., the origin in (1). Assume that the initial states associated with 2^D selected measurement segments can form all vertices of a *D*-dimensional parallelotope in the **x**-space, as illustrated in Fig. 3 for $D = 2$ by the parallelograms and rectangles. Then, after the linear transformation, these initial states should be able to form a hyperrectangle in the z-space. In other words, if the data set satisfies the symmetric condition in z-space after the linear transformation, it should consist of symmetrical pairs in x-space before the transformation. Therefore, the problem becomes identifying these symmetrical pairs in x-space.

However, from real-world measurements, it might not always be feasible to find an ideal *D*-dimensional parallelotope. Thus, the most symmetric set of initial states can be identified by solving this optimization problem:

$$\min_{\mathbf{x}_{A'}} \left\| \mathbf{x}_A + \mathbf{x}_{A'} \right\| \quad s.t. \ \left\| \mathbf{x}_A \right\|, \left\| \mathbf{x}_{A'} \right\| > r_{threshold}, \tag{6}$$

where the norm can take the Euclidian distance when state variables are considered to be the same type, $\mathbf{x}_A$ is the state vector in the set of initial states, and $\mathbf{x}_{A'}$ is its most symmetric peer in the set. A practical consideration in this context is the robustness against noise in measurements. The farther a measured state is from the origin, the less it is affected by noise. Therefore, it is advisable to select initial states that are not too close to the origin by defining their minimum distance, $r_{threshold}$, to the origin as specified in (6).

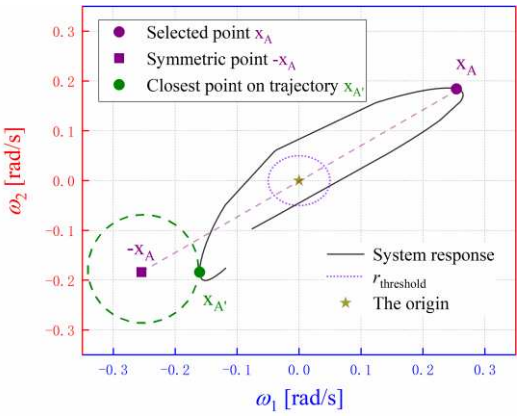

Fig. 2. The procedure to find a symmetric pair of initial states.

The process of identifying the most symmetric peer for a selected state is depicted in Fig. 2. Point $\mathbf{x}_A$ is selected along the trajectory, indicated by a purple circle, while its ideally symmetric state, $-\mathbf{x}_A$, is represented by a purple square; however, this point does not lie on the trajectory. Instead, another point, $\mathbf{x}_{A'}$, which is on the trajectory and closest to $-\mathbf{x}_A$ with the minimum distance $\|\mathbf{x}_A + \mathbf{x}_{A'}\|$, is identified as the solution to the optimization problem mentioned earlier. In this way, all such most symmetric pairs collectively approximate a parallelotope in the **x**-space. During Step 2, this parallelotope is transformed into an approximate hyperrectangle in **z**-space, ensuring the symmetric condition in **z**-space is met. In addition, to enhance the time performance, the KD tree approach [35] is also applied to search for the optimal symmetric pairs.

2) Step 2: Finding the transformation

The initial states are selected as symmetric pairs around the origin in the **x**-space, forming the vertices of a parallelotope. The next step involves identifying the transformation **H** that maps this parallelotope to a hyperrectangle. A method to determine the desired transformation is proposed in this step, which is exemplified for a two-dimensional system in Fig. 3.

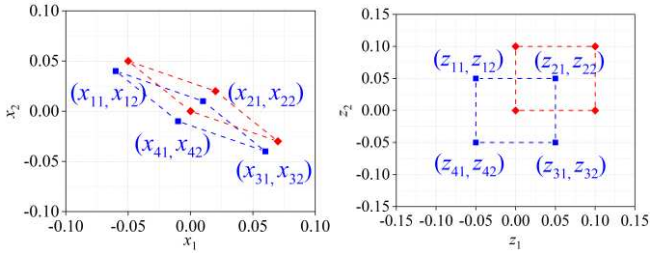

Fig. 3. The transformation of an initial state set.
(Left: Initial states in **x**-space. Right: Initial states in **z**-space)

The initial state set optimized in *Step 1* forms the blue parallelogram centered at the origin, as depicted in Fig. 3 (left). This parallelogram can be transformed into the red parallelogram by shifting the center to one of its vertices. Subsequently, a transformation is applied to convert the red parallelogram into the red rectangle shown in Fig. 3 (right), which is then translated back to the original origin. It becomes clear that the transformation from the red parallelogram to the red rectangle can be determined based on the edges of the parallelogram in x-space, as detailed below:

$$\begin{bmatrix} z_{i1} \\ z_{i2} \end{bmatrix} = \begin{bmatrix} x_{11}-x_{41} & x_{31}-x_{41} \\ x_{12}-x_{42} & x_{32}-x_{42} \end{bmatrix}^{-1} \begin{bmatrix} x_{i1} \\ x_{i2} \end{bmatrix} = \mathbf{H} \begin{bmatrix} x_{i1} \\ x_{i2} \end{bmatrix}, \quad (7)$$

where x_i is the initial state set in **x**-space, and z_i is the initial state in **z**-space. The translations to a new origin in **x**-space (from the blue parallelogram to the red parallelogram) and back to the original origin in **z**-space (from the red rectangle to the blue rectangle) effectively cancel each other out. Consequently, the desired transformation from **x**-space to **z**-space (from the blue parallelogram to the blue rectangle) remains unchanged as **H**. In other words, **H** is invariant following a coordinate translation. This observation is valid for an *N*-dimensional system, as demonstrated by Lemma 1 in the Appendix, where detailed proof of this property is also provided. This characteristic can be formally stated as a theorem that a transformation from a parallelotope in **x**-space to a hyperrectangle in **z**-space that are both centered at the origin of the dimension *N* can be determined from any *N*+1 pairs of vertices in **x**-space, denoted by $\{\mathbf{x_0}, \mathbf{x'_0}\}$, $\{\mathbf{x_1}, \mathbf{x'_1}\}$, …, $\{\mathbf{x_N}, \mathbf{x'_N}\}$, as $\mathbf{H}=[\mathbf{x_1}-\mathbf{x_0}, \ldots, \mathbf{x_N}-\mathbf{x_0}]^{-1}$.

3) Steps 3 and 4: Computing MPFs in z- and x-spaces

After determining the parameters of the linear transformation in the previous subsection, the trajectory in the **x**-space can also be transformed into the **z**-space. The B_{ki} values in **z**-space are obtained using Prony's analysis [26]. In **z**-space, the symmetric condition is met, enabling the computation of EPFs using (4). It is important to note that if a black-box model is employed, the first three steps can be ignored, and the MPFs in the **x**-space can be directly calculated. This method serves as an extension of the response-based approach, with details available in [26].

Theoretically, if all modes and their shapes or compositions are known, the calculation of MPFs becomes straightforward, given the established inverse relationship between the matrices made by right and left eigenvectors [36]

$$\mathbf{P} = \mathbf{\Phi} \circ \mathbf{\Psi}^{\mathrm{T}} = \mathbf{\Phi} \circ \mathbf{\Phi}^{-\mathrm{T}}, \quad (8)$$

where "∘" is Hadamard product.

Therefore, if the shapes and compositions of all modes can be determined from wide-area measurements, PFs can be directly computed. However, achieving full modal observability of the system is often not feasible due to insufficient phasor measurement units (PMUs) [37]. In fact, grid operators focus the real-time monitoring on selected dominant modes and thus do not have to pursue full modal observability. The MPFs are calculated as follows with subscripts *x* and *z* distinguishing **x**- and **z**-spaces.

$$\mathbf{PF}_z = \mathbf{\Phi}_z \circ \mathbf{\Psi}_z^{\mathrm{T}} = (\mathbf{H}\mathbf{\Phi}_x) \circ (\mathbf{H}^{-\mathrm{T}}\mathbf{\Psi}_x^{\mathrm{T}}), \quad (9a)$$

$$\mathbf{PF}_x = \mathbf{\Phi}_x \circ \mathbf{H}^{\mathrm{T}}[\mathbf{PF}_z / (\mathbf{H}\mathbf{\Phi}_x)]. \quad (9b)$$

With partial modal observability, $\mathbf{\Phi}_z$ is only partially known, so the MPFs in the **x**-space cannot be obtained directly. Consequently, the MPFs in the **x**-space cannot be directly determined. Assuming that the transformation **H** from **x**-space to **z**-space has been obtained in Step 3, these relationships can be derived for elements of matrices $\mathbf{\Phi}_x$ and Ψ_x:

$$[\mathbf{\Phi}_x]_{ij} = [\mathbf{H}^{-1}\mathbf{\Phi}_z]_{ij} = \sum_{k=1}^{N} m_{ik}\phi_{z,kj}, \quad (10a)$$

$$[\mathbf{\Psi}_x]_{ij} = [\mathbf{\Psi}_z\mathbf{H}]_{ij} = \sum_{k=1}^{N} h_{ki}\psi_{z,jk}. \quad (10b)$$

where h_{ki} and m_{ik} are the elements of the transformation matrix **H** and its inverse. Therefore, the PF for *i* state in *j* mode in **x**-space is

$$p_{x,ij} = \phi_{x,ij}\psi_{x,ji} = \sum_{k=1}^{N} m_{ik}\phi_{z,kj} \sum_{k=1}^{N} h_{ki}\psi_{z,jk}. \quad (11)$$

From the definition of PFs, there is

$$p_{x,ij} = \sum_{k=1}^{N} m_{ik}\phi_{z,kj} \sum_{k=1}^{N} h_{ki} \frac{p_{z,kj}}{\phi_{z,kj}}. \quad (12)$$

which associates MPFs in the **x**-space with corresponding mode shapes. In other words, if the right eigenvectors of certain modes in **z**-space are known, their corresponding MPFs in **x**-space can also be estimated after a linear transformation, even if the shapes and compositions of other modes are unknown.

C. Error Estimation

If the linearized model of the system is available, an error index on the EPFs can be calculated according to (5):

$$e_1 = \frac{1}{L} \sum_{l=1}^{L} \sum_{j=1, j\neq k}^{N} \psi_{jk}\phi_{ki} \frac{x_{j0}^{(l)}}{x_{k0}^{(l)}}. \quad (13)$$

Also, the following error index is introduced to evaluate the accuracy of the proposed MPFs compared to model-based PFs:

$$e_{2ij} = \left(\frac{\mathrm{PF}_j / \mathrm{PF}_i}{\mathrm{MPF}_j / \mathrm{MPF}_i} - 1 \right) \times 100\%, \quad (14)$$

where the subscripts *i* and *j* are the generator numbers of interest, respectively.

III. Case Studies

This section first illustrates the proposed measurement-based approach for PF estimation on a two-area system, considering both full and partial observabilities. Penetration of inverter-based resources (IBRs) is also considered. Then, it is tested on the NPCC 48-machine system with both ideal and practical measurements.

A. Two-area system study

A modified Kundur's two-area system [38] is used with generator inertias adjusted to present three distinct oscillatory modes at frequencies of 0.593Hz, 1.110Hz and 1.628Hz. The system includes generators 1 and 2 in Area 1, and generators 3 and 4 in Area 2. The 0.593 Hz mode is the inter-area mode, while the 1.110 Hz mode and 1.628 Hz mode are the intra-area modes of areas 1 and 2, respectively.

The mode compositions, mode shapes and PFs with four generators are computed from the model with respect to the inter-area mode. Fig. 4 presents a comparison of the results,

revealing that generator 3 displays the most important role in the mode shape. Meanwhile, generator 1 contributes more significantly to the composition of the mode than any other generator. In summary, generator 1 exhibits the largest PF when considering both the mode shape and its composition. From this example, it can be concluded that PFs serve as reliable indicators for ranking generators according to their bidirectional associations with the mode.

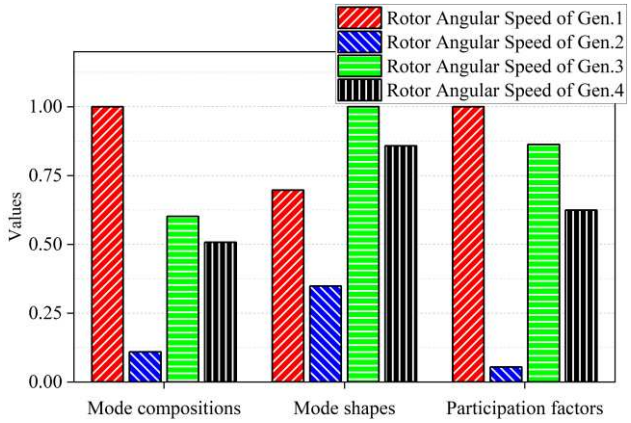

Fig. 4. Mode composition, shape and PF for rotor speed on the interarea mode

1) Assuming full observability

Assuming that all four generators are monitored by PMUs, a database of measurements is created using simulation results on four rotor speeds under approximately 12 disturbances. Fig. 5 (left) displays measurements of the four speeds in two different 3D projections to depict the measurements in their 4D space. Fig. 5 (middle and bottom) depicts some symmetric states identified in the **x**-space, which approximately form a 3-parallelotope, and their transformation approximately forms a cuboid in the **z**-space. The points labelled A, B, C, D, E, F, G, etc., in the middle figure of Fig. 5 represent symmetric states identified in the x-space, a subset of the system. In the bottom figure of Fig. 5, the transformed vertices are labelled A', B', C', D', E', F', G', and H'.

TABLE II compares the MPFs calculated from the proposed PF estimation approach with the model-based PFs, which are found to be very similar. The errors in the estimation can be attributed to two factors: 1) the most symmetric initial states in **x**-space may not perfectly form a parallelotope (as evident in Fig. 5. 2) errors in the estimation due to Prony's analysis in **z**-space. Simulation results confirm that if the initial states selected from measurements form a perfectly symmetric parallelotope, the MPFs will be an exact match to the PFs. It is worth noting that when the black-box model is available and the disturbance can be designed, the MPF proposed approach is almost identical to the PFs.

In this section, a sub-space strategy for PF estimation is also proposed and tested on the same two-area system. The strategy involves identifying three 2-parallelotopes using six symmetric pairs of generators and calculating relative MPFs for each parallelotope. The MPFs are then normalized to obtain the MPFs for each generator. The results are shown in TABLE III, where the MPFs for the two local modes at 1.110 Hz and 1.628 Hz accurately match the PFs, while the MPFs for the inter-area mode at 0.593 Hz have larger errors but still reflect a similar ranking of the PFs. Therefore, the sub-space strategy is more suitable for PF estimation of local modes. However, for inter-area modes, the reduction in dimension needs to balance the trade-off between accuracy and computational complexity.

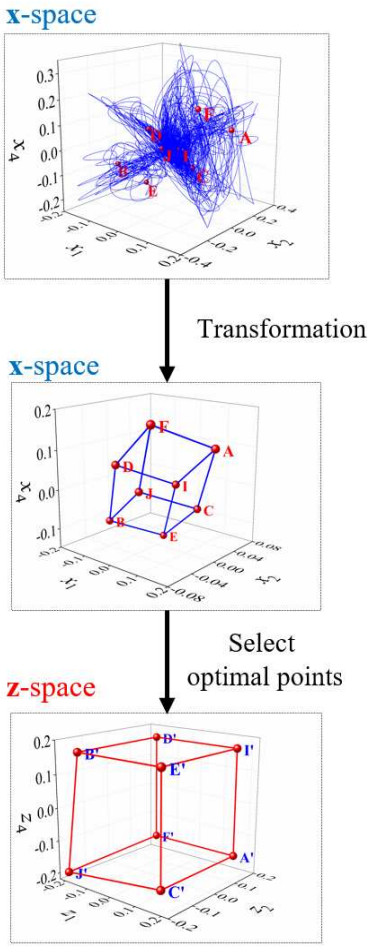

Fig. 5. The trajectory of response and selected initial states in state space (top - trajectories of generators 1, 2, and 3; middle - selected initial points before transformation; bottom - selected initial points after transformation)

TABLE II
THE PFS AND MPFS FOR FULL OBSERVABILITY STUDY

Generator	0.593 Hz		1.110 Hz		1.628 Hz	
	PFs	MPFs	PFs	MPFs	PFs	MPFs
1	1.00	1.00	2.0×10^{-3}	2.6×10^{-3}	0.13	0.13
2	0.06	0.06	6.2×10^{-4}	5.0×10^{-3}	1.0	1.0
3	0.86	0.90	0.80	0.82	2.9×10^{-3}	2.5×10^{-3}
4	0.62	0.66	1.00	1.00	8.3×10^{-3}	9.2×10^{-3}

TABLE III
THE PFS AND MPFS BASED ON THE RATIO OF THE TWO-DIMENSION SYSTEM

Generator	0.593 Hz		1.110 Hz		1.628 Hz	
	PFs	MPFs	PFs	MPFs	PFs	MPFs
1	1.00	1.00	2.0×10^{-3}	4.8×10^{-4}	0.13	0.12
2	0.06	0.17	6.2×10^{-4}	3.6×10^{-3}	1.00	1.00
3	0.86	1.06	0.80	0.62	2.9×10^{-3}	5.9×10^{-3}
4	0.62	0.97	1.00	1.00	8.3×10^{-3}	7.5×10^{-3}

2) Assuming partial observability

In this study, assume that not all generators are monitored by PMUs, and the state variables of unmeasured generators contain random changes following a uniform distribution. This research examines four distinct cases, with details provided in TABLE IV.

Case 1: Generators 1, 2 and 3 are monitored by PMUs, and the measurements of their speeds of the best symmetry are found. Generator 4, not monitored by a PMU, is assumed to have an initial speed change randomly from -0.02 to 0.02 rad/s.

Case 2: The same as Case 1 except that generator 3 also has a random initial speed as generator 4.

Case 3: The same as Case 1 except for an increased range of random initial speeds of generators 3 and 4.

Case 4: The same as Case 2 except for an increased range of random initial speeds of generators 3 and 4.

TABLE IV
THE DISTRIBUTION OF THE INITIAL STATE SET

Case	generator 1	generator 2	generator 3	generator 4
1	Symmetric	Symmetric	Symmetric	[-0.02 0.02]
2	Symmetric	Symmetric	[-0.02 0.02]	[-0.02 0.02]
3	Symmetric	Symmetric	Symmetric	[-0.1 0.1]
4	Symmetric	Symmetric	[-0.1 0.1]	[-0.1 0.1]

The study utilizes the error estimation presented in (14) to evaluate the performance of partial observability for generators 1 and 2, with the results outlined in TABLE V. A comparison between Cases 1 and 2, as well as Cases 3 and 4, indicates an increase in error as more generators lack PMU equipment. Additionally, a rise in the distribution range of generator 4 results in an increase in error, as evident in Cases 2 and 4. The error of the 1.110 Hz mode is significantly higher due to the critical roles played by generators 3 and 4, particularly in cases where the latter is not equipped with a PMU. Overall, the accuracy of the estimated MPF can be significantly enhanced if the initial speed variance of a generator without a PMU is small, particularly when it contributes significantly to the mode(s) of interest. Consequently, MPFs estimation demonstrates superior accuracy when more generators are equipped with PMUs.

TABLE V
THE ERROR INDEX OF GENERATOR 1 VS. 2

Case	0.593 Hz	1.110 Hz	1.628 Hz
1	0.78%	5.66%	0.35%
2	-1.51%	7.23%	1.02%
3	-0.82%	12.67%	1.04%
4	-1.65%	48.13%	1.97%

3) Considering penetration of IBRs

Another case study was conducted on the two-area system, replacing Generators 2, 3, and 4 by IBRs. The detailed model of the IBR can be found in [39] and [40]. Twelve disturbances were considered, and the results are shown in TABLE VI.

In this study, the system with three synchronous generators is treated as a new two-area system. Although the topology remains the same, the swing equation and the Phase-Locked Loop (PLL) equation are different.

Due to the penetration of IBRs, the frequencies of the modes become much faster. The inter-area mode is around 1.05 Hz, while the local modes are around 1.95 Hz and 2.22 Hz. The MPFs are closely aligned with the PFs, although Gen 3 and Gen 4 exhibit relatively larger errors. This discrepancy arises because the two IBRs are located far from the synchronous generators, and the coherence between these two generators is more pronounced. The differences are notable for Gen 1 and 2, making it easier to distinguish between them.

TABLE VI
THE PFS AND MPFS FOR FULL OBSERVABILITY STUDY

Generator	1.05 Hz		1.95Hz		2.22 Hz	
	PFs	MPFs	PFs	MPFs	PFs	MPFs
1	0.83	0.82	0.51	0.49	2.5×10^{-3}	1.9×10^{-2}
2	0.51	0.37	1.00	1.00	3.6×10^{-3}	8.6×10^{-2}
3	1.00	1.00	1.6×10^{-2}	0.11	0.57	0.72
4	0.60	0.48	4.3×10^{-3}	0.24	1.00	1.00

B. NPCC System

Next, the proposed approach's performance is tested on a much larger NPCC 140-bus 48-machine system, as illustrated in Fig. 6. Two distinct measurement datasets will be generated: random initial states and faults. For this large system, there are more than 200 modes based on the system model. However, the 0.6 Hz inter-area mode, with its low damping ratio, is the dominant mode. The analysis will focus on five generators (21, 24, 26, 27, and 78) that have the largest participation factors for this 0.6 Hz inter-area mode.

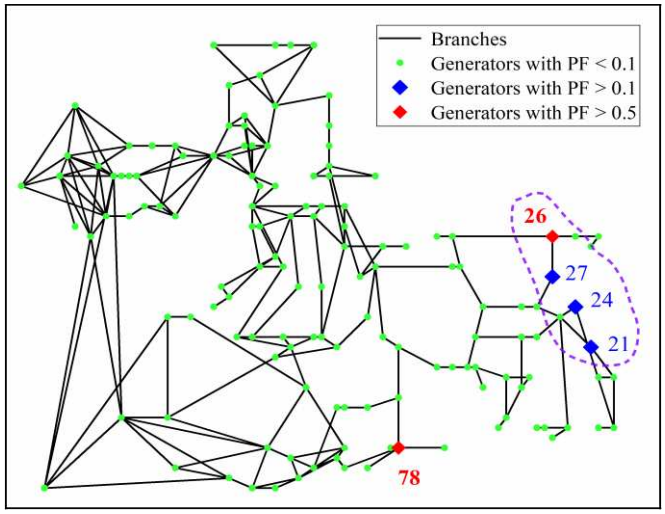

Fig. 6. Topology of the NPCC 140-bus system

1) Test on faults.

This test simulates 50 three-phase faults on the lines near one end in the New England region of the system, as shown in Fig. 6. Each fault lasts 50 ms before being cleared, and no generator or line is tripped after the fault. A total of 50 fault simulations will be executed to generate the measurement dataset, which will then be used to estimate MPFs. The outcomes of the test will be presented in TABLE VII.

From the results, only the MPFs of generators 78 and 26 are close to their true values. The MPFs of the remaining three generators are inaccurate due to the strong coherence observed among the last four generators in the oscillation. The highest mutual coherence of 0.98 is observed between the columns formed by generators 24 and 21, with condition number 249. Consequently, the sampling matrix is ill-conditioned, significantly amplifying the input error. A detailed proof of the relationship between error and coherence can be found in the appendix.

TABLE VII
THE PFS BASED ON FAULT SIMULATIONS

Generator	78	26	24	21	27
(True) PFs	1.00	0.54	0.43	0.18	0.10
MPFs	0.99	0.61	1.00	0.88	0.31

4) Test on random initial states.

Based on the findings from the two-area system study, it is established that the performance of the proposed approach is significantly influenced by the distribution of initial states within the measurement dataset. To validate this observation on the NPCC system, a measurement dataset will be generated by conducting simulations of scenarios starting from randomly selected initial states within the state space. The selected initial states will be sufficiently disturbed within the state space. A total of 50 scenarios will be generated, each simulating for 20 seconds, resulting in the measurement dataset.

The MPFs estimated using data from 10, 20, 30, 40, and all 50 simulations are presented in TABLE VIII. The results indicate that utilizing data from 20 simulations can correctly identify the generator with the largest PF. Increasing the number of simulations to 40 results in the correct ranking of PFs. When all 50 scenarios are applied, the MPFs closely match the true PFs, thus demonstrating the effectiveness of the measurement-based PF approach for the large NPCC system.

TABLE VIII
THE PFS BASED ON RANDOM INITIAL STATES

Generator	True PFs	MPFs based on several scenarios				
		10	20	30	40	50
78	1.00	0.95	1.00	1.00	1.00	1.00
26	0.54	0.99	0.50	0.61	0.60	0.55
24	0.43	1.00	0.42	0.75	0.36	0.40
21	0.18	0.13	0.17	0.50	0.25	0.17
27	0.10	0.12	0.25	0.72	0.15	0.16

To study how IBR penetration may influence the performance of the proposed approach, three IBRs are respectively connected to the buses of three highly participating generators, i.e. 26, 24 and 21. The MPFs estimated using data from 10, 20, 30, 40, and all 50 simulations are presented in Table IX. Note that the added IBRs, have changed the system model as well as model-based participation factors. The case study shows that all 50 scenarios are applied, the new MPFs still match well the true PFs calculated from the new system model with IBRs. Therefore, the increase in IBR penetration has not affected the estimation of participation factors for generators.

TABLE IX
THE PFS BASED ON RANDOM INITIAL STATES WITH THREE IBRS INSTALLED

Generator	True PFs	MPFs based on several scenarios				
		10	20	30	40	50
78	1.0	0.86	1.00	1.00	1.00	1.00
26	0.41	1.00	0.50	0.42	0.53	0.44
24	0.17	0.45	0.31	0.18	0.31	0.15
21	0.13	0.11	0.35	0.13	0.21	0.13
27	0.04	0.07	0.28	0.11	0.06	0.07

C. Discussion of the proposed Approach

Several factors influence the performance of the proposed approach, with system nonlinearity being the most significant. The method assumes linear system behavior, but nonlinearity becomes more prominent under heavy load conditions or large disturbances, reducing the accuracy of participation factor estimation with the Prony analysis. Specifically, nonlinearity affects the calculations in (4) and propagates through to the final results. To address this, extended Prony analysis can be applied, as it accounts for nonlinear dynamics and allows for more accurate oscillation behavior estimation, especially near resonance. Additionally, techniques like squeezing wavelet transformation can help isolate and analyze nonlinear components, further improving robustness.

Measurement noise also affects the accuracy of PF estimation. As shown in (13), noise on key generators (e.g., generators 78 and 26 in the NPCC system) significantly impacts results, while noise on less critical generators (e.g., generator 45) has a smaller effect. To mitigate noise, methods such as the matrix pencil method, Kalman filtering, and other noise-reduction techniques can be employed, improving the accuracy of PF estimations by reducing the noise in the measurements.

IV. CONCLUSION

This paper has developed a measurement-based approach for PF estimation. The computed MPFs are the best approximations of the model-based theoretical PFs by means of a linear coordinate transformation that relaxes the symmetric condition for calculating PFs from responses of the system. The efficacy of the proposed approach is demonstrated through its applications to both small- and large-scale power system models with discussions on its error.

APPENDIX

A. The invariant of transformation

Lemma 1 The transformation from a parallelotope to a hyperrectangle of the same dimension is invariant under a translation of coordinates.

Proof: Assume the **x**-space is a vector space with basis $\{\mathbf{u}_1, \ldots, \mathbf{u}_N\}$. Since **z**-space is a vector space transformed from the **x**-space by transformation **H**. Thus, $\{\mathbf{v}_1, \ldots, \mathbf{v}_N\}$ is a set of basis in **z**-space with $\mathbf{v_j}=\mathbf{Hu_j}$ (j=1, …, N). For a random translation $\mathbf{s}_{\mathbf{x},\mathbf{0}}$ with coordinate $[s_1, \ldots, s_N]^T$ in **x**-space, it can be noticed that

$$\mathbf{H}\mathbf{s}_{x,0} = \mathbf{H}\sum_{j=1}^{N} s_j \mathbf{u}_j = \sum_{j=1}^{N} s_j \mathbf{H}\mathbf{u}_j = \sum_{j=1}^{N} s_j \mathbf{v}_j = \mathbf{s}_{z,0}. \quad (14)$$

Hence, for a random initial state in **x**-space,

$$\mathbf{H}(\mathbf{x}_i - \mathbf{s}_{x,0}) = \mathbf{H}\mathbf{x}_i - \mathbf{H}\mathbf{s}_{x,0} = \mathbf{z}_i - \mathbf{s}_{z,0}. \quad (15)$$

Therefore, for any $\mathbf{x_i}$ with translation $\mathbf{s_{x,0}}$ in $\mathbf{x}$-space will be transformed by $\mathbf{H}$ to the initial state $\mathbf{z_i} = \mathbf{Hx_i}$ with the translation $\mathbf{s_{z,0}} = \mathbf{Hs_{x,0}}$ in $\mathbf{z}$-space. In other words, $\mathbf{H}$ is invariant under a translation of coordinates.

First, translate the origin to one of the N+1 vertices, say $\mathbf{x_0}$. Vectors $\mathbf{x_1}$-$\mathbf{x_0}$, …, $\mathbf{x_N}$-$\mathbf{x_0}$ together define a convex polyhedral cone as well as a set of basis vectors [41]. Thus, for any of these vectors $\mathbf{x_i}$-$\mathbf{x_0}$, there is

$$\mathbf{x}_i - \mathbf{x}_0 = \sum_{j=1}^{N} a_j(\mathbf{x}_j - \mathbf{x}_0) \quad a_j = \{0,1\}. \quad (16)$$

It is easy to notice that if let $\mathbf{z_i}$-$\mathbf{z_0}$= $[a_1, \ldots, a_N]^{-1}$, there is

$$\mathbf{H}^{-1}(\mathbf{z}_i - \mathbf{z}_0) = \sum_{j=1}^{N} a_j(\mathbf{x}_j - \mathbf{x}_0) = \mathbf{x}_i - \mathbf{x}_0. \quad (17)$$

Because a_j takes only 0 or 1 for any j, $\mathbf{z_i}$ -$\mathbf{z_0}$ is actually the vertex on the hyperrectangle. Thus, $\mathbf{H}$ maps vertices of the N-parallelotope in $\mathbf{x}$-space after the translation to vertices of a hyperrectangle in $\mathbf{z}$-space. Also, since $\mathbf{H}$is linear and invertible with a zero kernel, it is injective. Thus, all 2^N vertices on the N-parallelotope can be transformed by $\mathbf{H}$ to the 2^N unique vertices on the hyperrectangle.

Besides, from *Lemma 1,* the translation to $\mathbf{x_0}$ does not change $\mathbf{H}$, so H is the desired transformation.

■

B. The relationship between coherence and error

The proposed approach can be represented as solving a linear equation in the following form:

$$\mathbf{S\Psi} = \mathbf{B}, \quad (18)$$

where $\mathbf{S}$ is the sampling matrix of measurements, with each row representing the rotor speed data of all generators (at different columns) at a particular time instant of the measuring window. $\mathbf{\Psi}$ is the mode composition that needs to be computed, while $\mathbf{B}$ represents the excitation energy calculated from the measurement. Given a sufficiently high sampling frequency of measurements, $\mathbf{S}$ generally has significantly more rows than columns, making (19) an overdetermined system.

However, if the rotor speeds of two generators (say generators i and j) are almost proportional to each other, the columns i and j of S become coherent, meaning that these two vectors are nearly linearly dependent. This results in a large condition number of $\mathbf{S}$ and a considerable error in the solution of (19). The coherency index γ of $\mathbf{S}$ is defined as

$$\gamma = \max_{1\le\alpha\le N, 1\le\beta\le N} \left\|\mathbf{s}_\alpha^{\mathrm{T}}\mathbf{s}_\beta\right\| / \left(\left\|\mathbf{s}_\alpha\right\|\left\|\mathbf{s}_\beta\right\|\right) = \left\|\mathbf{s}_i^{\mathrm{T}}\mathbf{s}_j\right\| / \left(\left\|\mathbf{s}_i\right\|\left\|\mathbf{s}_j\right\|\right), \quad (19)$$

where $\mathbf{s}_\alpha$ and $\mathbf{s}_\beta$ are arbitrary two-column vectors of the matrix $\mathbf{S}$, and $\mathbf{s}_i$ and $\mathbf{s}_j$ are two-column vectors that have the smallest angle in between. The condition number of a matrix is typically defined by using its nearest lower-rank matrix [42].

$$\mathrm{cond}(\mathbf{S}) = \max \left\|\mathbf{S}\right\|_2 / \left\|\mathbf{S} - \hat{\mathbf{S}}\right\|_2, \mathrm{cond}(\mathbf{S}) = \max \left\|\mathbf{S}\right\|_2 / \left\|\mathbf{S} - \hat{\mathbf{S}}\right\|_2, \quad (20)$$

The 2-norm of a matrix is the square root of the sum of all its elements squared. Consider some matrix $\hat{\mathbf{S}}$ that is the same as $\mathbf{S}$ except that column j equals its column i. Namely,

$$\hat{\mathbf{S}} = [\mathbf{s}_1, \quad \ldots, \quad \mathbf{s}_{j-1}, \quad \mathbf{s}_i, \quad \mathbf{s}_{j+1}, \quad \ldots, \quad \mathbf{s}_N]. \quad (21)$$

It has a lower rank reduced by 1. From (21),

$$\mathrm{cond}(\mathbf{S}) \ge \frac{\left\|\mathbf{S}\right\|_2}{\left\|\mathbf{S} - \hat{\mathbf{S}}\right\|_2} = \frac{\left\|\mathbf{S}\right\|_2}{\left\|\mathbf{s}_i - \mathbf{s}_j\right\|_2} = \frac{\left\|\mathbf{S}\right\|_2}{\sqrt{\left|\mathbf{s}_i\right|^2 + \left|\mathbf{s}_j\right|^2 - 2\left|\mathbf{s}_i\right|\left|\mathbf{s}_j\right|\gamma}}. \quad (22)$$

Thus when $\gamma \to 1$, there is

$$\left\|\mathbf{s}_i\right\|^2 + \left\|\mathbf{s}_j\right\|^2 - 2\left\|\mathbf{s}_i\right\|\left\|\mathbf{s}_j\right\|\gamma \to 0 \quad \mathrm{cond}(\mathbf{S}) \to \infty, \quad (23)$$

which means that the condition number will become extremely large. Since the sampling matrix is ill-conditioned, errors will become inevitable.

REFERENCES

[1] B. Wang, K. Sun, "Location methods of oscillation sources in power systems: a survey," *J. Modern Power Syst. Clean Energy*, vol. 5, no. 2, pp. 151-159, March 2017.

[2] X. Xu, W. Ju, B. Wang, K. Sun, "Real-Time Damping Estimation on Nonlinear Electromechanical Oscillation," *IEEE Trans. Power Syst.*, vol. 36, no. 4, pp. 3142-3152, July 2021.

[3] S. Liu, et al., "A Normal Form Analysis Approach to Siting Power System Stabilizers (PSSs) and Assessing Power System Nonlinear Behavior," *IEEE Trans. Power Syst.*, vol. 21, no. 4, pp. 1755-1762, Oct. 2006

[4] Y. Li, L. Fan, Z. Miao, "Wind in Weak Grids: Low-Frequency Oscillations, Subsynchronous Oscillations, and Torsional Interactions," *IEEE Trans. Power Syst.*, vol. 35, no. 1, pp. 109-118, Jan. 2020.

[5] J. Liu, W. Yao, et al., "Impact of Power Grid Strength and PLL Parameters on Stability of Grid-Connected DFIG Wind Farm," *IEEE Trans. Sustain. Energy*, vol. 11, no. 1, pp. 545-557, Jan. 2020.

[6] G. Tzounas, F. Milano, "On the Emulation of Synchronous Machine Dynamics by Converter-Interfaced Generators," *IEEE PES General Meeting*, Orlando, FL, USA, 2023, pp. 1-5.

[7] H. Liu, X. Xie, et al., "Subsynchronous Interaction Between Direct-Drive PMSG Based Wind Farms and Weak AC Networks," *IEEE Trans. Power Syst.*, vol. 32, no. 6, pp. 4708-4720, Nov. 2017.

[8] L. Wang, D. Yang, et al., " Synchronized-ambient-data-driven participation-factor-based generation rescheduling strategy for enhancing the damping level of interconnected power systems," *I. J. Electrical Power & Energy Syst.*, vol. 146, no. 1, Mar. 2023.

[9] J. Duan, D. Shi, et al., "Deep-Reinforcement-Learning-Based Autonomous Voltage Control for Power Grid Operations," *IEEE Transactions on Power Systems*, vol. 35, no. 1, pp. 814-817, Jan. 2020.

[10] Y. Zhan, et al, "Frequency-Domain Modal Analysis of the Oscillatory Stability of Power Systems with High-Penetration Renewables," *IEEE Trans. Sustain. Energy*, vol. 10, no. 3, pp. 1534-1543, July 2019.

[11] Y. Zhu, Y. Gu, Y. Li, T. C. Green, "Participation Analysis in Impedance Models: The Grey-Box Approach for Power System Stability," *IEEE Trans. Power Syst.*, vol. 37, no. 1, pp. 343-353, Jan. 2022.

[12] D. Yang, Y. Sun, "SISO Impedance-Based Stability Analysis for System-Level Small-Signal Stability Assessment of Large-Scale Power Electronics-Dominated Power Systems," *IEEE Trans. Sustain. Energy*, vol. 13, no. 1, pp. 537-550, Jan. 2022.

[13] G. Tzounas, et al, "Modal Participation Factors of Algebraic Variables," *IEEE Trans. Power Syst.*, vol. 35, no. 1, pp. 742-750, Jan. 2020.

[14] K. Li, et al, "Improvement of Electromechanical Mode Identification from Ambient Data with Stochastic Subspace Method," *IEEE PES Asia-Pac. Power Energy Eng. Conf.*, Macao, China, 2019, pp. 1-6.

[15] B. Wang, K. Sun, "Formulation and Characterization of Power System Electromechanical Oscillations," *IEEE Trans. Power Syst.*, vol. 31, no. 6, pp. 5082-5093, Nov. 2016.

[16] J. Zhang, et al, "A Novel SVC Allocation Method for Power System Voltage Stability Enhancement by Normal Forms of Diffeomorphism," *IEEE Trans. Power Syst.*, vol. 22, no. 4, pp. 1819-1825, Nov. 2007.

[17] E. Abed, D. Lindsay, W. Hashlamoun: "On participation factors for linear systems", *Automatica*, vol. 36, no. 10, pp. 1489-1496, Oct. 2000

[18] R. A. Ramos, A. G. M. Moraco, T. C. C. Fernandes and R. V. de Oliveira, "Application of extended participation factors to detect voltage fluctuations in distributed generation systems," *IEEE Power and Energy Society General Meeting*, Detroit, MI, USA, 2011, pp. 1-6.

[19] E. L. Geraldi, et al, "An approach for statistical quantitative analysis of voltage fluctuations using extended participation factors," *IEEE PES General Meeting*, Denver, CO, USA, 2015, pp. 1-5.

[20] W. A. Hashlamoun, et al, "New Results on Modal Participation Factors: Revealing a Previously Unknown Dichotomy," *IEEE Trans. Automatic Control*, vol. 54, no. 7, pp. 1439-1449, July 2009.

[21] B. Hamzi, E. Abed, "Local modal participation analysis of nonlinear systems using Poincaré linearization," *Nonlinear Dynamics*, vol. 99, no. 1, pp. 803-811, Jan. 2020.

[22] A. B. Iskakov, "Definition of State-in-Mode Participation Factors for Modal Analysis of Linear Systems," *IEEE Trans. Automatic Control*, vol. 66, no. 11, pp. 5385-5392, Nov. 2021.

[23] B. She, F. Li, H. Cui, J. Zhang, R. Bo, "Fusion of Microgrid Control With Model-Free Reinforcement Learning: Review and Vision," *IEEE Trans. Smart Grid*, vol. 14, no. 4, pp. 3232-3245, July 2023

[24] M. Netto, Y. Susuki, L. Mili, "Data-Driven Participation Factors for Nonlinear Systems Based on Koopman Mode Decomposition," *IEEE Control Systems Letters*, vol. 3, no. 1, pp. 198-203, Jan. 2019.

[25] P. Sharma, V. Ajjarapu, U. Vaidya, "Data-Driven Identification of Nonlinear Power System Dynamics Using Output-Only Measurements," *IEEE Trans. Power Syst.*, vol. 37, no. 5, pp. 3458-3468, Sept. 2022.

[26] M. Sajjadi et al., "Estimation of Participation Factors Using the Synchrosqueezed Wavelet Transform," *IEEE PES General Meeting*, Orlando, FL, USA, 2023, pp. 1-5.

[27] S. Zhao, K. A. Loparo, "Forward and Backward Extended Prony (FBEP) Method for Power System Small-Signal Stability Analysis," *IEEE Trans. Power Syst.*, vol. 32, no. 5, pp. 3618-3626, Sept. 2017

[28] M. Ruan, et al, "Improved Prony Method for High-Frequency-Resolution Harmonic and Interharmonic Analysis," *IEEE 2nd Intl. Conf. Electronics Technology*, Chengdu, China, 2019.

[29] T. K. Ram, S. Krishna, "Accuracy of Normal Form Approximation for Power System Nonlinear Analysis," *IEEE Trans. Power Syst.*, vol. 36, no. 5, pp. 4828-4831, Sept. 2021

[30] M. Zghal, L. Mevel, P. Del Moral, "Modal parameter estimation using interacting Kalman filter," *Mechanical Systems and Signal Processing*, vol. 47, no. 1, pp. 139-150, August 2014

[31] R. Diversi, et al, "Kalman filtering in extended noise environments," *IEEE Trans. Automatic Control*, vol. 50, no. 9, pp. 1396-1402, Sept. 2005

[32] A. Tavighi, et al, "Time-Window-Based Discrete-Time Fourier Series for Electromagnetic Transients in Power Systems," *IEEE Trans. Power Delivery*, vol. 33, no. 5, pp. 2551-2561, Oct. 2018,

[33] T. Jiang, et al, "Forced Oscillation Source Location of Bulk Power Systems Using Synchrosqueezing Wavelet Transform," *IEEE Trans. Power Syst.*, vol. 39, no. 5, pp. 6689-6701, Sept. 2024,

[34] T. Xia, Z. Yu, K. Sun, D. Shi, Z. Wang, "Extended Prony Analysis on Power System Oscillation Under a Near-Resonance Condition," *IEEE PES General Meeting*, Montreal, QC, Canada, 2020.

[35] M. Wu, K. Xie, G. Zeng, "Fast Search Algorithm of Nonlinear LUT Based on K-D Tree," *Intl. Conf. Comp. Sci. Appl.*, Wuhan, China, 2013.

[36] P. Kundur, *Power System Stability and Control*. McGraw-Hill, 1993.

[37] J. F. Hauer, C. J. Demeure, L. L. Scharf, "Initial results in Prony analysis of power system response signals," *IEEE Trans. Power Syst.*, vol. 5, no. 1, pp. 80-89, Feb. 1990.

[38] J. J. Sanchez-Gasca et al., "Inclusion of higher order terms for small-signal (modal) analysis: committee report-task force on assessing the need to include higher order terms for small-signal (modal) analysis," *IEEE Trans. Power Syst.*, vol. 20, no. 4, pp. 1886-1904, Nov. 2005.

[39] Z. Zhou, et al, "Small Signal Stability of Phase Locked Loop Based Current-Controlled Inverter in 100% Inverter-Based System," *IEEE Trans. Sustain. Energy*, vol. 14, no. 3, pp. 1612-1623, July 2023

[40] W. Wang, et al, "Transient stability analysis and stability margin evaluation of phase-locked loop synchronised converter-based generators," *IET Gener. Transm. Distrib.*, vol. 14 no. 22, pp. 5000–5010, 2020.

[41] J. J. Sanchez-Gasca et al., "Inclusion of higher order terms for small-signal (modal) analysis: committee report-task force on assessing the need to include higher order terms for small-signal (modal) analysis," *IEEE Trans. Power Syst.*, vol. 20, no. 4, pp. 1886-1904, Nov. 2005

[42] B. Datta, *Numerical Methods for Linear Control Systems*. Elsevier, 2004.

Tianwei Xia (Member, IEEE) received his B.S. degree in electrical engineering from China Agricultural University, Beijing, China, in 2014, his M.S. degree in electrical engineering from the University of Chinese Academy of Sciences, Beijing, China, in 2017, and his Ph.D. degree in electrical engineering from the University of Tennessee, Knoxville, TN, USA, in 2023. He is currently a planning engineer at Dominion Energy, Richmond, VA, USA. His research interests include power system planning, renewable energy integration, dynamic system responses and data analytics.

Zhe Yu (Senior Member, IEEE) received the B.E. degree from Tsinghua University, Beijing, China, in 2009, the M.S. degree from Carnegie Mellon University, Pittsburgh, PA, USA, in 2010, and the Ph.D. degree in electrical engineering from Cornell University, Ithaca, NY, USA, in 2016. He joined Ant Group in 2024. His research interests include deep learning, causal inference, time-series forecasting, and optimization.

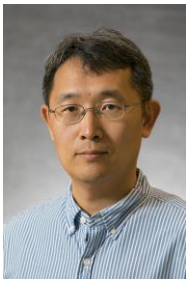

Kai Sun (Fellow, IEEE) is a Professor in the Department of Electrical Engineering and Computer Science at the University of Tennessee, Knoxville, USA. He received his B.S. degree in Automation in 1999 and his Ph.D. degree in Control Science and Engineering in 2004, both from Tsinghua University, Beijing, China. From 2007 to 2012, he served as a project manager for R&D projects in grid operations, planning, and renewable integration at the Electric Power Research Institute (EPRI), Palo Alto, CA.

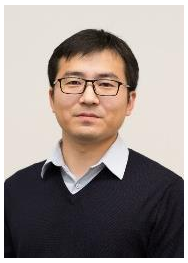

Di Shi (Senior Member, IEEE) received his Ph.D. in Electrical Engineering from Arizona State University, Tempe, AZ, USA, in 2012. He is currently an Associate Professor in the Klipsch School of Electrical and Computer Engineering at New Mexico State University. His research interests focus on power system dynamics, operation and control, as well as the application of AI and machine learning in power systems.

Kaiyang Huang (Graduate Student Member, IEEE) received the B.S. degree in electrical engineering from North China Electric Power University, China, in 2020. He is currently pursuing the Ph.D. degree at the Department of Electrical Engineering and Computer Science, University of Tennessee, Knoxville, USA. His research interests include power system simulation, transient stability analysis, and dynamics.